ESC European Society of Cardiology

European Heart Journal Open (2024) **4**, 1–13
https://doi.org/10.1093/ehjopen/oead128

ORIGINAL ARTICLE
Translational basic science

Mapping microarchitectural degeneration in the dilated ascending aorta with *ex vivo* diffusion tensor imaging

Mofei Wang[1,2,†], Justin A. Ching-Johnson[1,3,†], Hao Yin[1], Caroline O'Neil[1], Alex X. Li[1], Michael W.A. Chu[4,5], Robert Bartha[1,3], and J. Geoffrey Pickering [1,2,3,5,6,*]

[1]Robarts Research Institute, Schulich School of Medicine and Dentistry, Western University, 1151 Richmond St. N. London, Canada, N6A 5B7; [2]Department of Biochemistry, Western University, 1151 Richmond St. N. London, Canada, N6A 3K7; [3]Department of Medical Biophysics, Western University, 1151 Richmond St. N. London, Canada, N6A 3K7; [4]Department of Surgery, Western University, 1151 Richmond St. N. London, Canada, N6A 3K7; [5]London Health Sciences Centre, 339 Windermere Rd, London, Ontario, Canada, N6A 5A5; and [6]Department of Medicine, Western University, 1151 Richmond St. N. London, Canada N6A 3K7

Received 12 May 2023; revised 26 October 2023; accepted 30 November 2023; online publish-ahead-of-print 5 December 2023

Handling Editor: Daniel F.J. Ketelhuth

Aims

Thoracic aortic aneurysms (TAAs) carry a risk of catastrophic dissection. Current strategies to evaluate this risk entail measuring aortic diameter but do not image medial degeneration, the cause of TAAs. We sought to determine if the advanced magnetic resonance imaging (MRI) acquisition strategy, diffusion tensor imaging (DTI), could delineate medial degeneration in the ascending thoracic aorta.

Methods and results

Porcine ascending aortas were subjected to enzyme microinjection, which yielded local aortic medial degeneration. These lesions were detected by DTI, using a 9.4 T MRI scanner, based on tensor disorientation, disrupted diffusion tracts, and altered DTI metrics. High-resolution spatial analysis revealed that fractional anisotropy positively correlated, and mean and radial diffusivity inversely correlated, with smooth muscle cell (SMC) and elastin content ($P < 0.001$ for all). Ten operatively harvested human ascending aorta samples (mean subject age 61.6 ± 13.3 years, diameter range 29–64 mm) showed medial pathology that was more diffuse and more complex. Nonetheless, DTI metrics within an aorta spatially correlated with SMC, elastin, and, especially, glycosaminoglycan (GAG) content. Moreover, there were inter-individual differences in slice-averaged DTI metrics. Glycosaminoglycan accumulation and elastin degradation were captured by reduced fractional anisotropy ($R^2 = 0.47$, $P = 0.043$; $R^2 = 0.76$, $P = 0.002$), with GAG accumulation also captured by increased mean diffusivity ($R^2 = 0.46$, $P = 0.045$) and increased radial diffusivity ($R^2 = 0.60$, $P = 0.015$).

Conclusion

Ex vivo high-field DTI can detect ascending aorta medial degeneration and can differentiate TAAs in accordance with their histopathology, especially elastin and GAG changes. This non-destructive window into aortic medial microstructure raises prospects for probing the risks of TAAs beyond lumen dimensions.

* Corresponding author. Tel: +1 519 663 3973, Fax: +1 519 434 3278, Email: gpickering@robarts.ca
† The first two authors contributed equally to the study.

Graphical Abstract

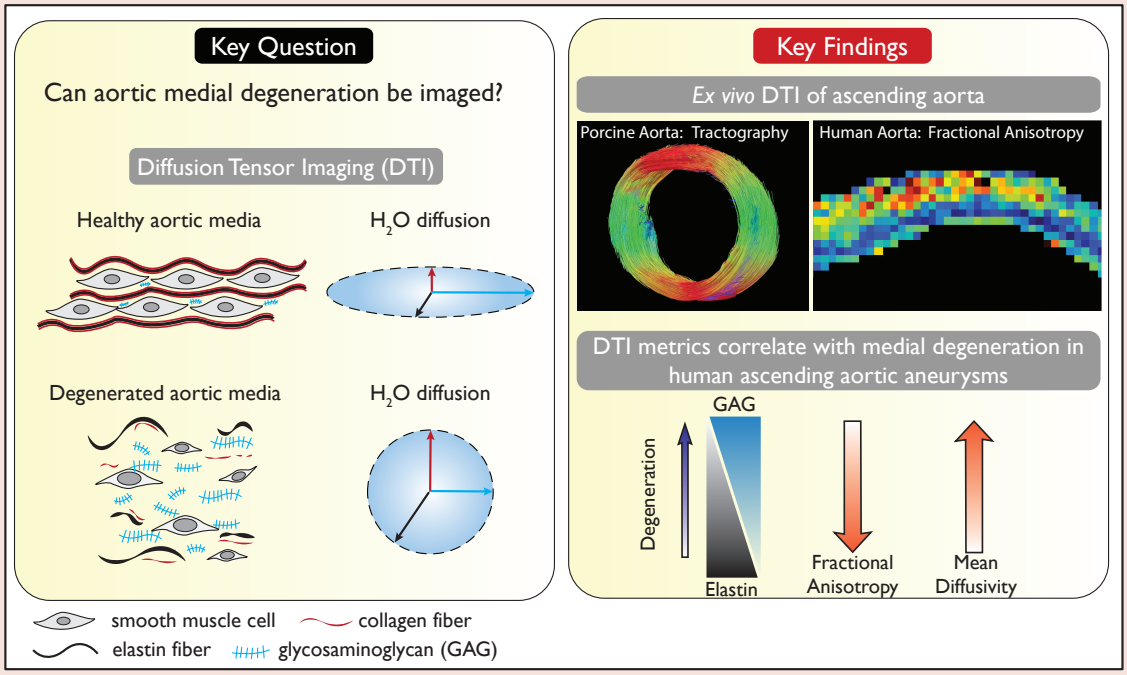

Keywords Ascending aortic aneurysm • Diffusion tensor imaging • Glycosaminoglycans • Elastin • Smooth muscle cells

Translational perspective

Ascending thoracic aortic aneurysms are at risk of dissecting, a frequently fatal outcome. The primary strategy for preventing this catastrophe is to monitor aortic diameter and surgically replace the involved segment once a size threshold has been reached. However, this approach is imperfect because many patients with acute dissection have aortic diameters below established thresholds for intervention. The current study establishes a strategy for quantitatively interrogating the microarchitecture of the degenerating and aneurysmal aortic wall. By informing on the pathology that weakens the aorta, diffusion tensor imaging may offer a new paradigm for evaluating the risk of dissection.

Introduction

Ascending thoracic aortic aneurysms (TAAs) carry the risk of catastrophic dissection and rupture.[1] The primary strategy for preventing these outcomes is to monitor aortic diameter and surgically replace the involved segment once a size threshold has been reached. However, optimally timing TAA surgery remains a challenge as more than half of patients with acute dissection have aortic diameters below established thresholds for intervention.[2–5] While lowering recommended size thresholds could circumvent this, it would also capture many individuals in the general population for whom aortic replacement would offer no benefit.[2,6] This dilemma highlights a need for better strategies to identify the high-risk ascending aorta.

Critical to the risk of ascending TAAs is the pathology within the media of the aortic wall. Whereas the normal aortic media has an organized layered structure, TAAs are characterized by elastin breakdown, loss and/or disarray of smooth muscle cells (SMCs), and accumulation of glycosaminoglycans (GAGs).[7,8] These changes are fundamental to aortic aneurysm formation and render the aortic wall mechanically vulnerable.[9–14] For this reason, strategies that report on medial architecture could provide critically important risk information beyond aortic dimensions.

Diffusion tensor imaging (DTI) is an advanced magnetic resonance imaging (MRI) acquisition method that produces image contrast based on the range and direction of the movement of water molecules. Tissue diffusion characteristics can be quantified using scalar metrics and diffusion paths displayed as tracts. Fractional anisotropy (FA) is a metric that describes the extent to which water movement is directionally oriented. Mean diffusivity (MD), another key metric, indicates the magnitude of diffusion averaged across x, y, and z axes, and radial diffusivity (RD) describes the magnitude of diffusion perpendicular to the long axis.

To date, DTI studies have focused primarily on the brain and spinal cord where diffusion in white matter pathways can be quantified and visualized using tractography.[15,16] However, data are emerging that the vessel wall is another substrate from which directional diffusion

data can be ascertained using DTI.[17–20] Moreover, DTI may have the capacity to be disease informing as atherosclerotic lesions have been shown to impact DTI signals.[21–23] Importantly, however, assessing the diseased aortic media of ascending TAAs is an imaging challenge because, unlike in atherosclerotic arteries, there is no new and bulky tissue added to the underlying artery wall. Instead, TAAs are characterized by changes in existing media with microstructure alterations that are comparatively modest. A strategy that could capture the range of disorder found specifically within the aortic media, and also detect patient-to-patient differences in medial microarchitecture, could be central to optimizing patient-specific TAA assessments.

To determine if degenerative disease changes in the ascending aortic media could be identified and characterized by DTI, we undertook *ex vivo* interrogation of ascending aortas and quantitatively compared DTI signals with the aortic wall constituents at high spatial resolution. We first modelled a degeneration spectrum in the porcine ascending aorta and then investigated 10 human ascending aortas harvested from patients at the time of surgery. Both intra-aorta and inter-subject relationships between DTI biomarkers and the compositional changes that underlie aortic wall vulnerability are assessed.

Methods

For full Methods, see Supplementary material online.

Porcine and human aorta preparations

Porcine aortas were harvested from 6-month-old Yorkshire pigs (Mount Brydges Abattoir, London, Ontario, Canada). To induce degenerative damage to the media, aortic segments were microinjected with 30 µL of a collagenase–elastase mixture. Aortic rings were then incubated at 37°C for 30 min, washed, and then incubated in M199 with 10% fetal bovine serum at 37°C for 15 h. Washed samples then underwent MRI.

Full-circumference human ascending aorta segments were harvested from 10 subjects, eight undergoing ascending aortic replacement for TAAs, one undergoing a Ross procedure for aortic stenosis, following written informed consent and in accordance with protocols approved by Western University Research Ethics Board (Project ID 5512), and one from an individual undergoing cardiac transplantation retrieved as normally discarded tissue with no patient identifiers. Maximal ascending aortic diameter was recorded from the double-oblique short-axis plane of contrast-enhanced multidetector computed tomography images. Samples were fixed with 10% neutral-buffered formalin within 30 min after resection for up to 21 days, prior to MRI.

Magnetic resonance imaging scanning and diffusion tensor imaging analysis

Images were acquired using a 31 cm horizontal bore 9.4 T MRI scanner (Agilent, Palo Alto, CA, USA) with a 15 cm gradient coil set of 450 mT/m strength and a Bruker Avance MRI III console running Paravision-6 software (Bruker BioSpin Corp, Billerica, MA; for further details, see Supplementary material online). Images were pre-processed using fMRI Software Library (FSL, v5.0.10, Oxford, UK), distortions corrected using the EDDY utility, and the DTIFIT toolkit was used to generate scalar metric maps for FA, MD, and RD and primary eigenvector direction. Tractography fibre modelling was undertaken with MRTRIX3[16] using a deterministic algorithm with an FA cut-off minimum of 0.1 and a maximum angle between successive steps of 30°. Seeds were placed using a rejection sampling algorithm, and a maximum of 5000 seeds were permitted per model.

Histological staining and regional analyses

Immediately after MR scanning, full-ring aortic specimens were placed in formalin, embedded in paraffin, and oriented as for the MR scanning. Full-ring 5 µm serial sections were stained with haematoxylin and eosin (H&E) and Movat's pentachrome stain and digitally scanned (Leica Aperio AT2 slide scanner, Lincolnshire, IL, USA).

Histological features were quantified in regions of interest (ROIs) selected using QuPath bioimage analysis software (v0.2.3).[24] For porcine aorta tissue sections, 90–120 ROIs (250 µm × 250 µm) were positioned with a minimum of 250 µm between adjacent ROIs to cover a sector of ~120° containing the damaged zone and adjacent uninjured aorta. For the human aorta sections, 30 equally distributed ROIs (250 µm × 250 µm) were positioned around the ring to sample the entire circumference and include inner, mid, and outer medial zones. To assess within-aorta signal variations, a radial profile analysis was undertaken using adjacent ROIs (300 µm × 300 µm) crossing the medial layer in two opposing regions of an aortic ring (total 28 ROIs).

Medial cell density was quantified from H&E-stained sections in sample-blinded manner using QuPath. Elastin and GAG area fractions were similarly quantified from segmented Movat's pentachrome-stained images after exporting to Fiji biological image analysis software (v1.53c).[25]

Histology–diffusion tensor imaging correlation

Whole-ring aorta tissue sections and the corresponding MRI slices were aligned using 3D Slicer (v4.11.0, Landmark Registration module) using a linear, non-rigid algorithm. An iodine mark at the aortic convexity for human aortas and aortic ring morphology features for both human and porcine aortas served as landmarks. Histologic data from ROIs were related to metrics from the corresponding voxels on the MRI maps. Variability in the user-defined alignment strategy was assessed by quantifying inter-observer agreement of the voxel-specific DTI metrics in two injured porcine aortic rings. This yielded good agreement among 217 ROIs/voxels with mean intra-class correlation coefficients of 0.84, 0.84, and 0.83 for FA, MA, and RD, respectively. For human ascending aortas with pathology, slice-averaged medial signals were studied using DTI metrics averaged from all voxels in the slice. These were compared with section-averaged elastin, GAG, and medial cell content.

Statistics

Descriptive statistics are reported as mean ± standard deviation (SD) for data passing the Shapiro–Wilk normality test (human aorta diameter) and median ± range for porcine histomorphometry, being of smaller sample size ($n = 4$). Comparison of DTI metrics in the porcine aortas between enzyme-injected sites, phosphate-buffered saline (PBS)-injected sites, and non-injection sites were undertaken using one-way analysis of variance with Tukey's multiple comparisons test. Intra-class correlation coefficients were compared based on a single-rating, absolute agreement, two-way random effects model using SPSS 25. Linear regression analyses were performed using GraphPad Prism (v.8.4, La Jolla, California, USA). Statistical significance was considered as $P < 0.05$, and absolute P-values are shown for $P \geq 0.0001$.

Results

Porcine model of aortic medial degeneration

To investigate if DTI could identify a range of degenerative changes in the ascending aortic media, we first developed a model of localized aortic wall damage. This entailed microinjecting an elastase–collagenase mixture into the media of ascending aortas harvested from 6-month-old Yorkshire pigs. This yielded localized medial destruction, evident with Movat's pentachrome and H&E staining, with damage spanning ~15% of the aortic ring circumference (*Figure 1*). In the outermost territories of disruption, lamellar units were still present but the elastin was frayed and SMCs were detached from the elastic laminae (*Figure 1B and C*). Closer to the injection site, elastin loss was more pronounced, and SMCs were more sparse and variably oriented. At the injection site, there was little to no elastin and only rare, shrunken SMCs (*Figure 1D and E*).

High-resolution digital quantification (90–120 ROIs per section) confirmed a graded and symmetrical profile of elastin and SMC loss

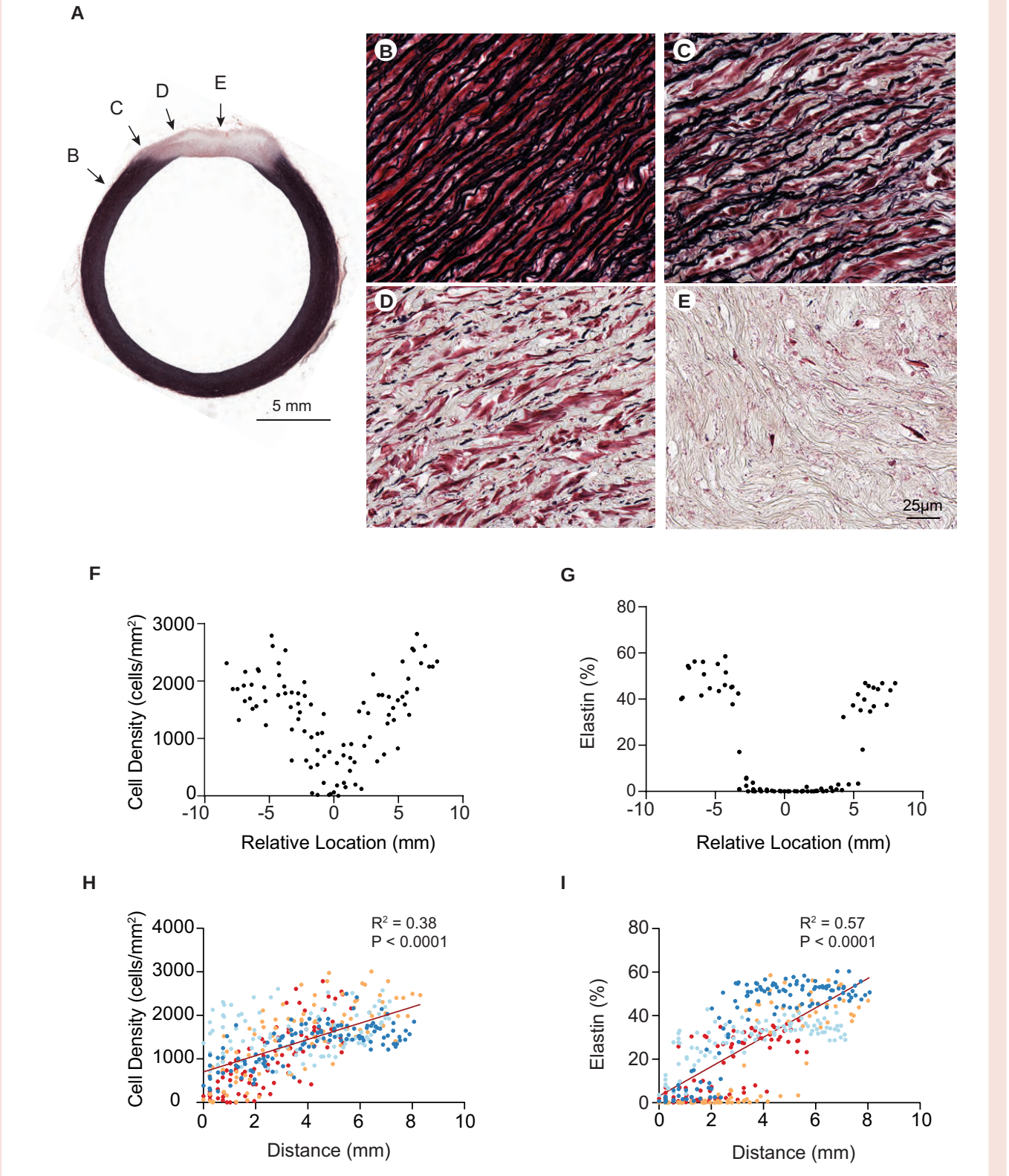

Figure 1 Medial degeneration in porcine ascending aorta subjected to enzyme microinjection. (*A*) Full circumference Movat's pentachrome-stained section of porcine ascending aorta showing local degeneration. (*B–E*) Higher magnification images corresponding to the sites shown in (*A*) depicting grades of medial degeneration, with progressive loss of elastin (black) and smooth muscle cells (red). (*F*, *G*) Plots of smooth muscle cell density (*F*) and elastin content (*G*) from individual regions of interest (250 μm × 250 μm) from a microinjected porcine aorta vs. the location relative to the micro-injection site, set as 0. (*H*, *I*) Regression analysis of SMC density and elastin content vs. absolute distance from the injection site. Data are from four individually injected aortas, denoted by the colours. The 90–120 regions of interest were studied per aorta.

(*Figure 1F* and *G*; Supplementary material online, *Figure S1*). Median SMC densities were 128 cells/mm^2 (range 0–688) in the digested territories and 2680 cells/mm^2 (2496–3008) in the non-digested territories. Median elastin area values were 0.36% (0–2.7) at the injection site and 50.0% (37.9–60.4) at non-digested territories ($n = 4$ aortas). Smooth muscle cell content and elastin content both positively correlated with distance from the injection site ($R^2 = 0.38$, $P < 0.0001$; $R^2 = 0.57$ $P < 0.0001$, *Figure 1H* and *I*). These findings thus establish a quantifiable model of localized and graded ascending aortic degeneration.

Diffusion tensor imaging of porcine ascending aortic degeneration

We next scanned control and enzyme-injected ascending aortic samples with MRI at a field strength of 9.4 T. Artefact-free diffusion tensor images (slice thickness of 500 μm) were obtained for full aortic rings. Colour maps of primary eigenvector orientations revealed organized, predominantly circumferential diffusion tensors in normal aortas. However, in enzyme-injected aortas, there was marked vector disarray in the region subjected to enzyme microinjection (*Figure 2A* and *B*). Regional aortic wall disorder was also detected by tractography, with otherwise primarily circumferential diffusion tracts disrupted at the site of injury (*Figure 2C*).

To quantify the diffusion attributes, we generated DTI scalar maps (*Figure 3A, C,* and *E*). In control aortas ($n = 4$), FA, MD, and RD were relatively homogeneous throughout the aortic media. However, for injured aortas ($n = 4$), FA was notably reduced at the site of the lesion and MD and RD were substantially increased. Plotting signals on a voxel-by-voxel basis vs. their absolute distance from the injection site revealed a relatively symmetrical profile of diffusion tensor signals, with FA lowest and MD and RD highest near the injection site (*Figure 3B, D,* and *F*). The respective signals progressively transitioned to normal values in the adjacent undamaged aortic regions. We also confirmed that the DTI changes were due to enzyme action on the tissue, rather than mechanical disruption from the needle and injected volume, by quantifying DTI signals in a separate set of aortic rings ($n = 4$) that were injected with enzyme mixture and equal volume PBS on opposite sides of the ring (see Supplementary material online, *Figure S2*).

Diffusion tensor scalar metrics correlate with elastin and smooth muscle cell content in the damaged ascending aorta

To determine if DTI scalar indices were associated with specific histopathologic features, ROI grids applied to digital histology images were positioned on co-aligned DTI metric maps from the same aortic ring for high-resolution data comparison. This revealed that FA positively correlated with SMC content. Twenty-seven per cent of the variance in FA could be explained by differences in SMC content. As well, MD and RD negatively correlated with cell content and 39% of the variance in MD and 42% of the variance in RD could be explained differences in SMC density ($P < 0.0001$ for all; see Supplementary material online, *Figure S3A–C*).

Linear relationships were also present between the diffusion metrics and elastin content. Here, 55% of the variance in FA, 49% of the variance in MD, and 60% of the variance in RD could be explained by differences in elastin content ($P < 0.0001$ for all; see Supplementary material online, *Figure S3D–F*). We also found that the DTI metric–histopathology relationships held using coarser spatial resolutions, akin to those of clinical imaging, as obtained by binning the voxel and ROI data (2×2 and 3×3; Supplementary material online, *Table S1*). Collectively, these findings establish that DTI-based assessments of the aorta both identified local wall degradation and also discriminated voxel-by-voxel diffusion variations in accordance with histology-defined composition.

Diffusion tensor imaging of human ascending aorta

We next sought to determine if DTI could inform on the more complex microarchitectures of human ascending aortas. We first explored DTI–compositional relationships by assessing the ascending aorta of a cardiac transplant recipient. A radial gradient of architectures existed, with relatively preserved lamellar units in the outer media but more disrupted elastin and SMC loss in the inner media, together with wide inter-lamellar spaces occupied by GAGs (*Figure 4A*). Remarkably, DTI scalar maps of the corresponding MRI slice also displayed heterogeneity. Fractional anisotropy was higher in the outer media and lower in the inner media, whereas MD and RD were relatively low in the outer media but high in the inner media (*Figure 4B*).

Quantifying compositional features in adjacent ROIs across the media, and DTI metrics in corresponding voxels, confirmed parallel or anti-parallel profiles. Smooth muscle cell density and elastin content progressively declined, and GAG content rose. Fractional anisotropy declined, and MA and RD rose (*Figure 4C*). Furthermore, quantifying six profiles across the media, including three from the opposite side of the aortic ring, revealed statistically significant correlations (*Table 1*). Interestingly, the most robust relationships were seen with GAG content (*Table 1* and *Figure 4D*). Here, 50% of the variance in FA, 53% of the variance in MD, and 52% of the variance in RD were attributed to changes in GAG content ($P < 0.0001$ for each). Coarsening the effective resolution by binning two adjacent voxels/ROIs across the profile showed that DTI metric correlations with GAG content persisted (see Supplementary material online, *Table S2*).

Diffusion tensor imaging can report on inter-individual differences in ascending aortic media composition

A desired attribute of imaging biomarkers is the ability to discriminate inter-individual differences. With this in mind, we studied an additional nine human ascending aortas, sequentially retrieved by intra-operative harvest from nine individuals. The clinical conditions were degenerative/sporadic TAA ($n = 5$), bicuspid aortic valve–associated TAA ($n = 2$), Loeys–Dietz syndrome 3 (LDS3) TAA ($n = 1$), and aortic stenosis (bicuspid aortic valve) managed with a Ross procedure ($n = 1$). Mean ascending aorta diameter was 49.9 ± 10.6 mm (range 29–64 mm). Subject demographics are provided in *Table 2*.

Aortas from all subjects showed medial degenerative changes, and the pathology was generally diffuse. Therefore, we evaluated slice-averaged DTI metrics as potential biomarkers of aortic media pathology. The slice-averaged FA ranged from 0.33 to 0.46, slice-averaged MD from 0.00069 to 0.00099 mm^2/s, and slice-averaged RD from 0.00053 to 0.00081 mm^2/s. Notably, differences in DTI signals could be appreciated visually between some aortas (Figure S4). This is illustrated in *Figure 5*, which depicts the ascending aorta from a 44-year-old individual with a bicuspid aortic valve undergoing a Ross procedure and that of a 54-year-old individual with LDS3. In neither case was the ascending aorta diameter substantially dilated (29 and 37 mm, respectively). However, the LDS3 aorta had a demonstrably lower FA and demonstrably higher MD.

We next quantified medial cell density, elastin content, and GAG content for each aorta and compared these with corresponding slice-averaged values for FA, MD, and RD. To our surprise, the DTI metrics did not correlate with SMC density (*Figure 6A*). However, FA strongly correlated with elastin content ($R^2 = 0.76$, $P = 0.002$, *Figure 6B*). As well, MD and RD inversely associated with elastin content ($R^2 = 0.18$ and 0.31, respectively), although not with statistical significance ($P = 0.26$ and 0.12). Even more striking were relationships between DTI metrics and GAG content. Fractional anisotropy was

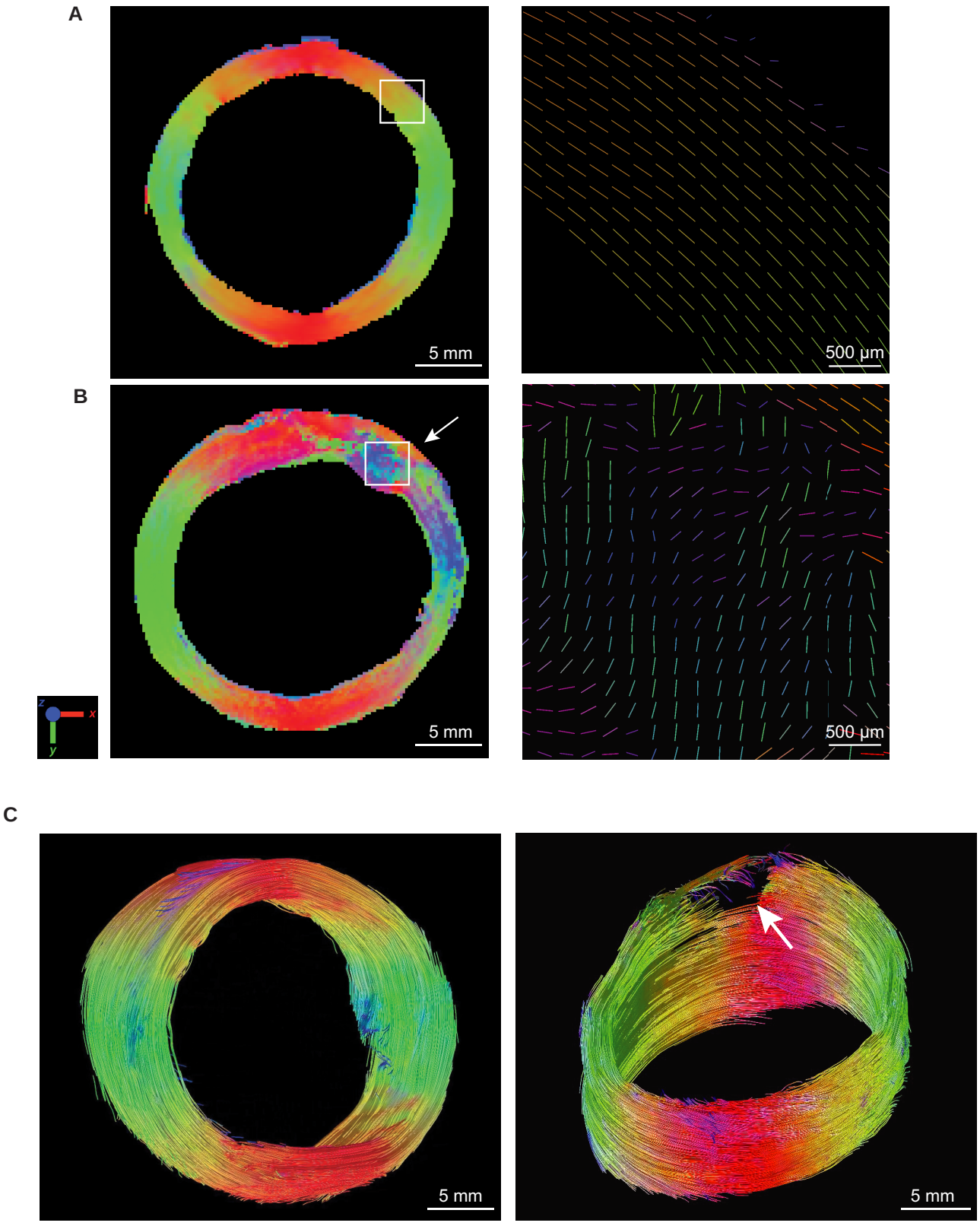

Figure 2 Eigenvector and tract depiction of normal and microinjected porcine ascending aortas. (*A*, *B*) Maps showing direction of eigenvectors in the media of normal (*A*) and microinjected (*B*) porcine ascending aortas subjected to diffusion tensor imaging at 9.4 T field strength. On the left, the dominant 3D orthogonal vector is colour mapped. On the right, 2D vector orientation and relative magnitude are displayed for each voxel. (*C*) 3D depiction of tracts for 2 cm segments of porcine ascending aortas. Local absence of tracts is evident for the enzyme-injected aorta at the site of injection (right, arrow).

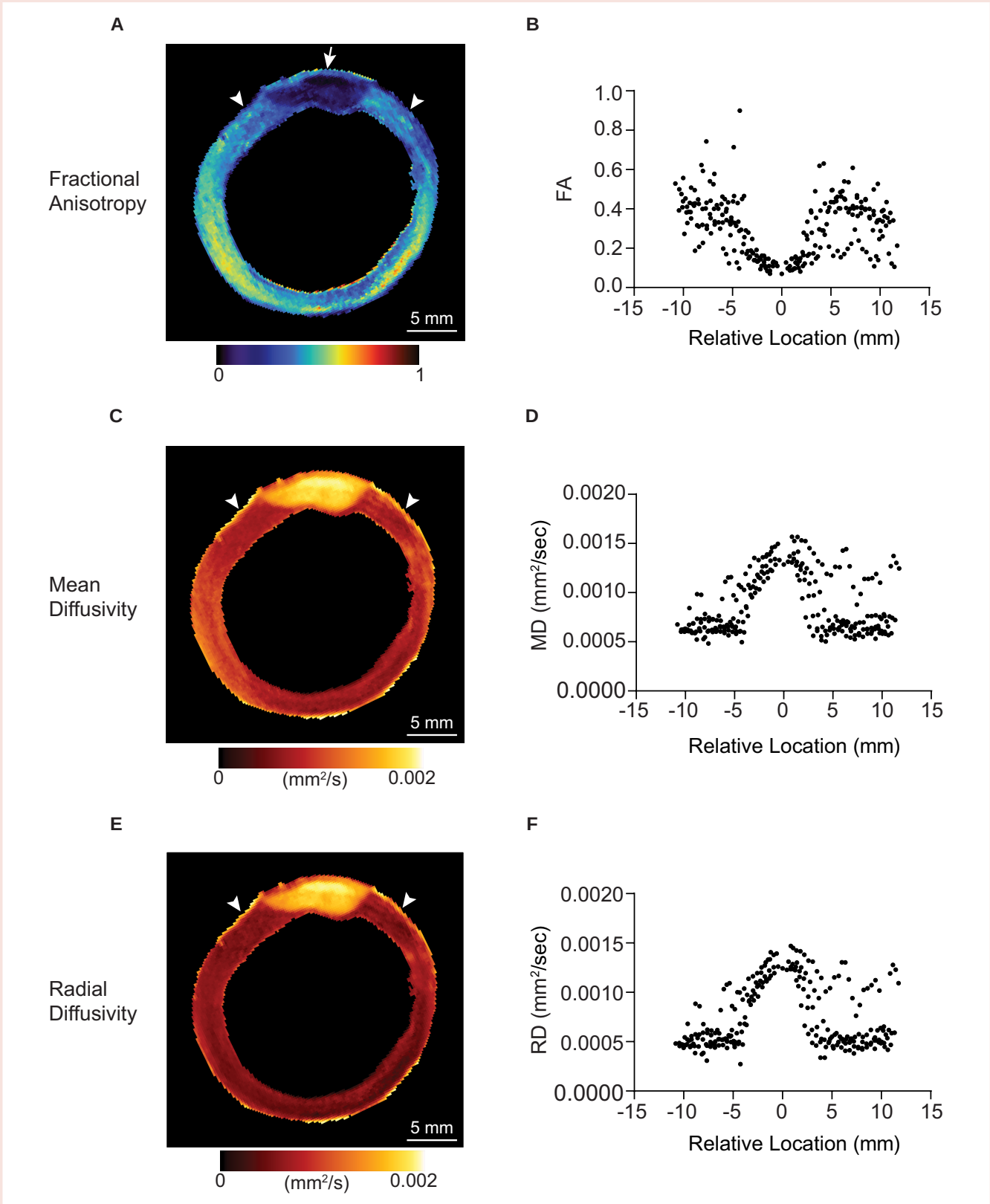

Figure 3 Diffusion tensor imaging scalar maps of enzyme-microinjected porcine ascending aorta. (*A–F*) Ascending aorta maps and spatial plots of diffusion metrics for fractional anisotropy (*A*, *B*), mean diffusivity (*C*, *D*), and radial diffusivity (*E*, *F*) for a 500 μm thick slice of porcine aorta subjected to collagenase–elastase microinjection and scanned at 9.4 T with diffusion tensor imaging. Arrow denotes the microinjection site, and arrowheads denote the borders within which the volumes of interest were quantified. Each data point in the plots denotes metrics from individual voxels (200 × 200 × 500 μm). FA, fractional anisotropy; MD, mean diffusivity; RD, radial diffusivity.

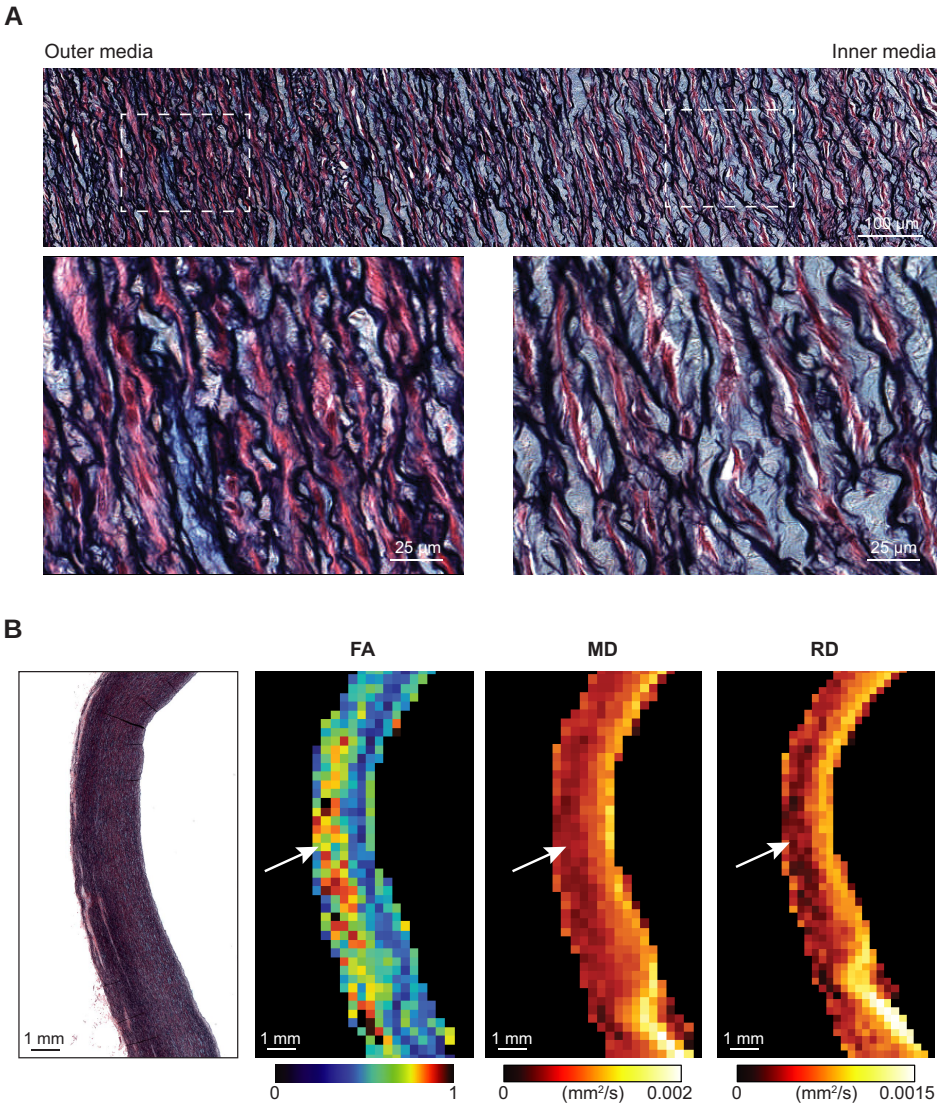

Figure 4 Gradients of degeneration and compositional changes within human aortic media revealed by diffusion tensor imaging. (*A*) Movat's pentachrome-stained section across the media width of ascending aorta of a heart transplant recipient. A profile of progressive degeneration from the outer to inner media can be seen. Zoomed images of regions in the dashed boxes are shown below, illustrating more fragmentation of elastin, accumulation of glycosaminoglycan, and loss of smooth muscle cells in the inner media. (*B*) Low-magnification section of the ascending aorta and corresponding maps of fractional anisotropy, mean diffusivity, and radial diffusivity. Outer to inner spatial differences in these diffusion tensor imaging - attributes can be seen, with lower anisotropy and greater mean and radial diffusion evident in the inner media. (*C*) Haematoxylin and eosin-stained and Movat's pentachrome-stained sections across the media of human ascending aorta with adjacent regions of interests (300 × 300 μm) demarcated and corresponding quantitative profile data from histological features and diffusion tensor imaging metrics. Each diffusion tensor imaging metric is derived from the corresponding voxel (300 × 300 × 500 μm) of the magnetic resonance imaging slice from which the tissue section was taken. (*D*) Scatter plots and linear regression data from six medial profiles of the aorta depicting the relationships between diffusion tensor imaging metrics and the histological attributes. $n = 30$ histology–diffusion tensor imaging data points from co-aligned images. FA, fractional anisotropy; MD, mean diffusivity; RD, radial diffusivity; GAG, glycosaminoglycan.

strongly inversely correlated with GAG content ($R^2 = 0.47$, $P = 0.043$, *Figure 6C*), whereas as MD ($R^2 = 0.46$, $P = 0.045$) and RD ($R^2 = 0.60$, $P = 0.015$) both positively correlated with GAG content. Neither the DTI metrics nor the histologically defined medial components correlated significantly with aortic diameter in this series of nine subjects (see Supplementary material online, *Table S3*).

These findings establish that inter-individual differences in the microstructure of the ascending aorta are distinguishable by DTI.

Discussion

In this *ex vivo* imaging study, we have established that DTI can provide critical information on the microstructure of the diseased ascending aortic wall. Studying both porcine and human ascending aortas, we found that DTI could (i) detect localized aortic medial damage; (ii) discriminate a range of medial changes and do so in accordance with histological changes; (iii) identify radial compositional heterogeneity in

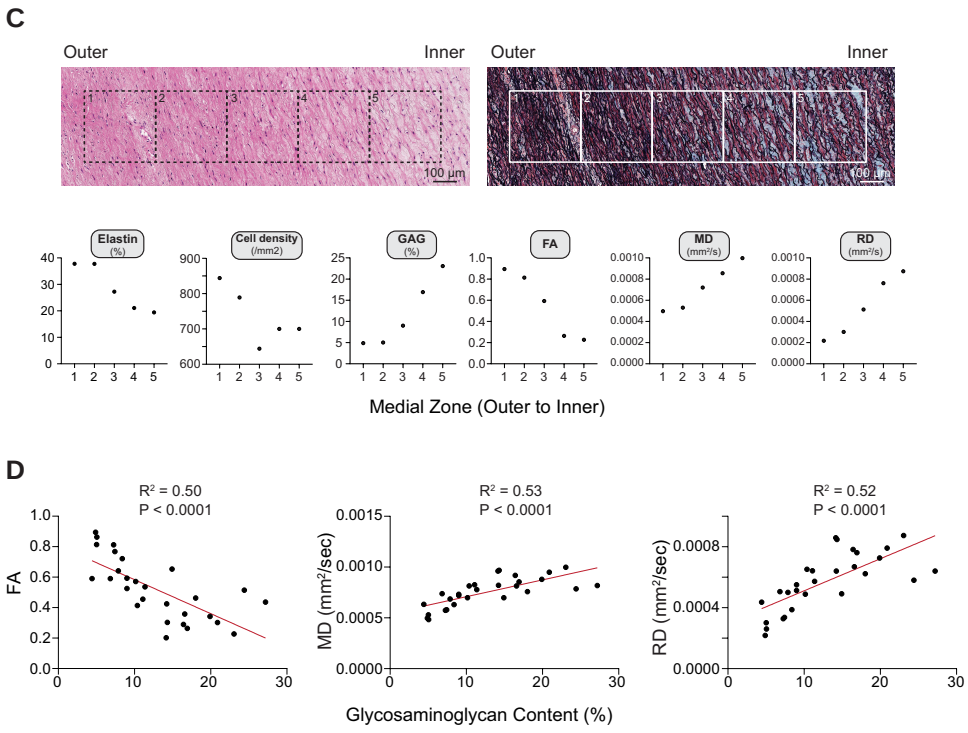

Figure 4 Continued

Table 1 Relationships between diffusion tensor imaging metrics and microstructure components across the media of human ascending aorta

	DTI metrics	*r*	R^2	*P*-value
Cell density	FA	0.41	0.17	0.028
	MD	−0.42	0.18	0.025
	RD	−0.42	0.18	0.027
Elastin	FA	0.54	0.29	0.0031
	MD	−0.46	0.21	0.007
	RD	−0.46	0.27	0.004
GAG	FA	−0.71	0.50	0.0001
	MD	0.73	0.53	0.0001
	RD	0.72	0.52	0.0001

GAG, glycosaminoglycan; FA, fractional anisotropy; MD, mean diffusivity; RD, radial diffusivity.

Table 2 Characteristics of patients with ascending aorta pathology

Patient	Age	Sex	Aetiology	Aortic lumen diameter (mm)
1	66	M	Bicuspid aortic valve	50
2	79	M	Sporadic/degenerative	64
3	80	M	Sporadic/degenerative	52
4	59	M	Sporadic/degenerative	55
5	71	M	Sporadic/degenerative	56
6	55	M	Bicuspid aortic valve	54
7	46	M	Sporadic/degenerative	52
8	54	M	Loeys–Dietz syndrome 3	37
9	44	F	Bicuspid aortic valve	29

human aortic media; and (iv) discriminate inter-subject differences in medial microstructure of ascending TAAs. Moreover, we established that there are multiple potential drivers of the altered DTI metrics in TAAs, with GAG content standing out as a particularly strong determinant.

We found circumferentially aligned diffusion tensors and coherent tract arrays in the normal porcine aortic media. These findings support that of others,[17,26] and they served as a foundation for investigating if DTI could interrogate pathological architectures. Microinjecting a collagenase–elastase mixture modelled two pathologies relevant to TAAs, SMC loss and elastin degradation. The resulting local lesions were reliably identified based on disoriented eigenvectors, terminated diffusion tracts, and altered diffusion metrics. Moreover, the severity of both elastin and SMC loss was tightly correlated with augmented diffusion rates (MD and RD) and loss of preferred directionality (FA).

This capacity of DTI to effectively grade medial degeneration held for human aortas. The outer-to-inner gradient of medial integrity, detected by quantitative shifts in FA, MD, and RD, was particularly noteworthy as such intra-medial detail is not detected with traditional imaging methodologies and may even be under-appreciated by routine histology. Interestingly, higher FA and lower MD in the outer medial zone has been reported for the porcine carotid artery, although histology was

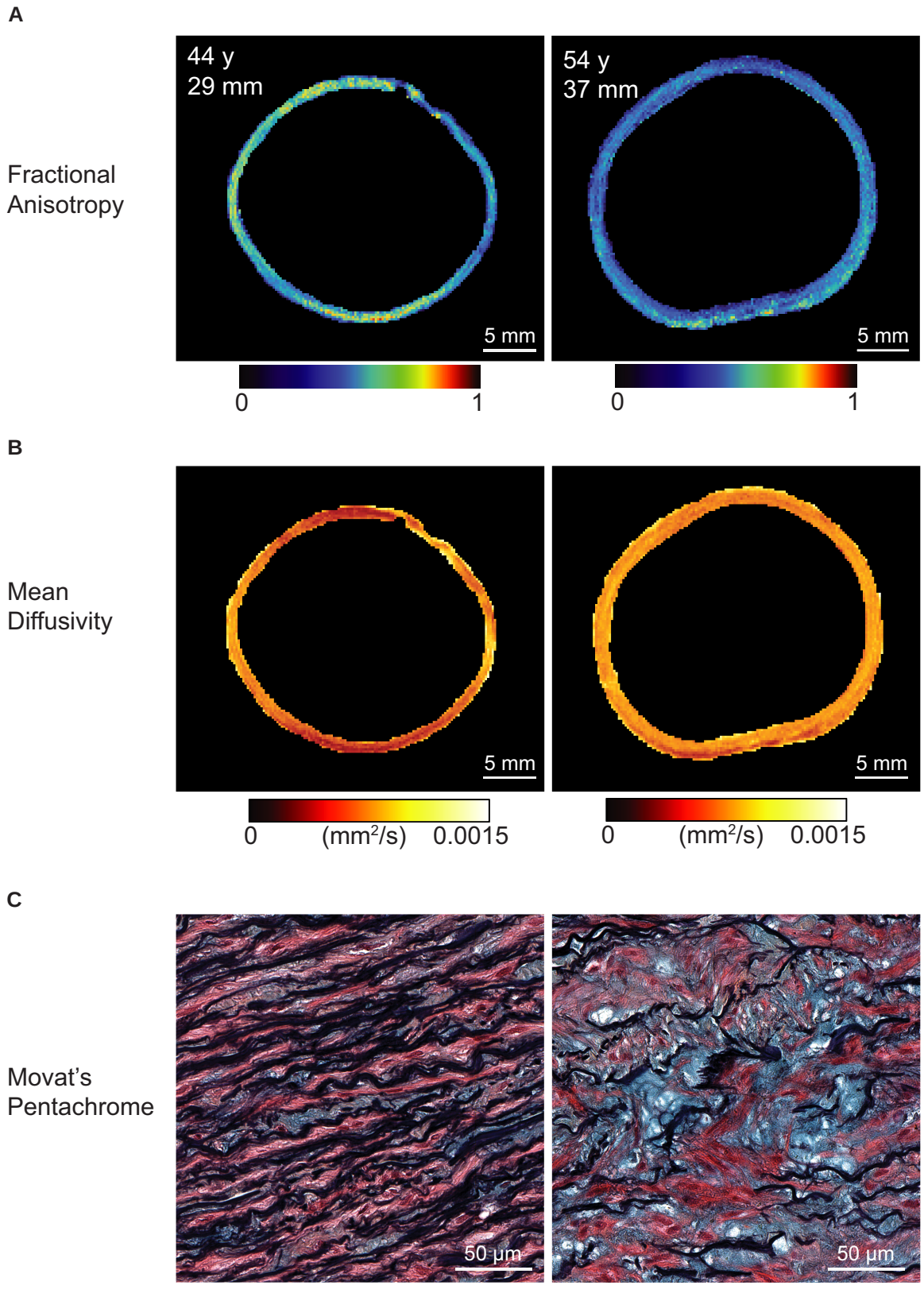

Figure 5 Inter-subject differences in diffusion tensor imaging–derived maps of fractional anisotropy and mean diffusivity. (*A*, *B*) Ascending aorta maps of fractional anisotropy (*A*) and mean diffusivity (*B*). The sample on the left is that of an aorta harvested from an individual undergoing a Ross procedure and that on the right of an individual with Loeys-Dietz syndrome 3. Visually appreciable and reciprocal differences between the diffusion tensor imaging maps for the two patient samples are evident. (*C*) Corresponding sections stained with Movat's pentachrome showing disrupted elastin, disoriented smooth muscle cells, and an accumulation of glycosaminoglycans in the Loeys-Dietz syndrome 3 aorta.

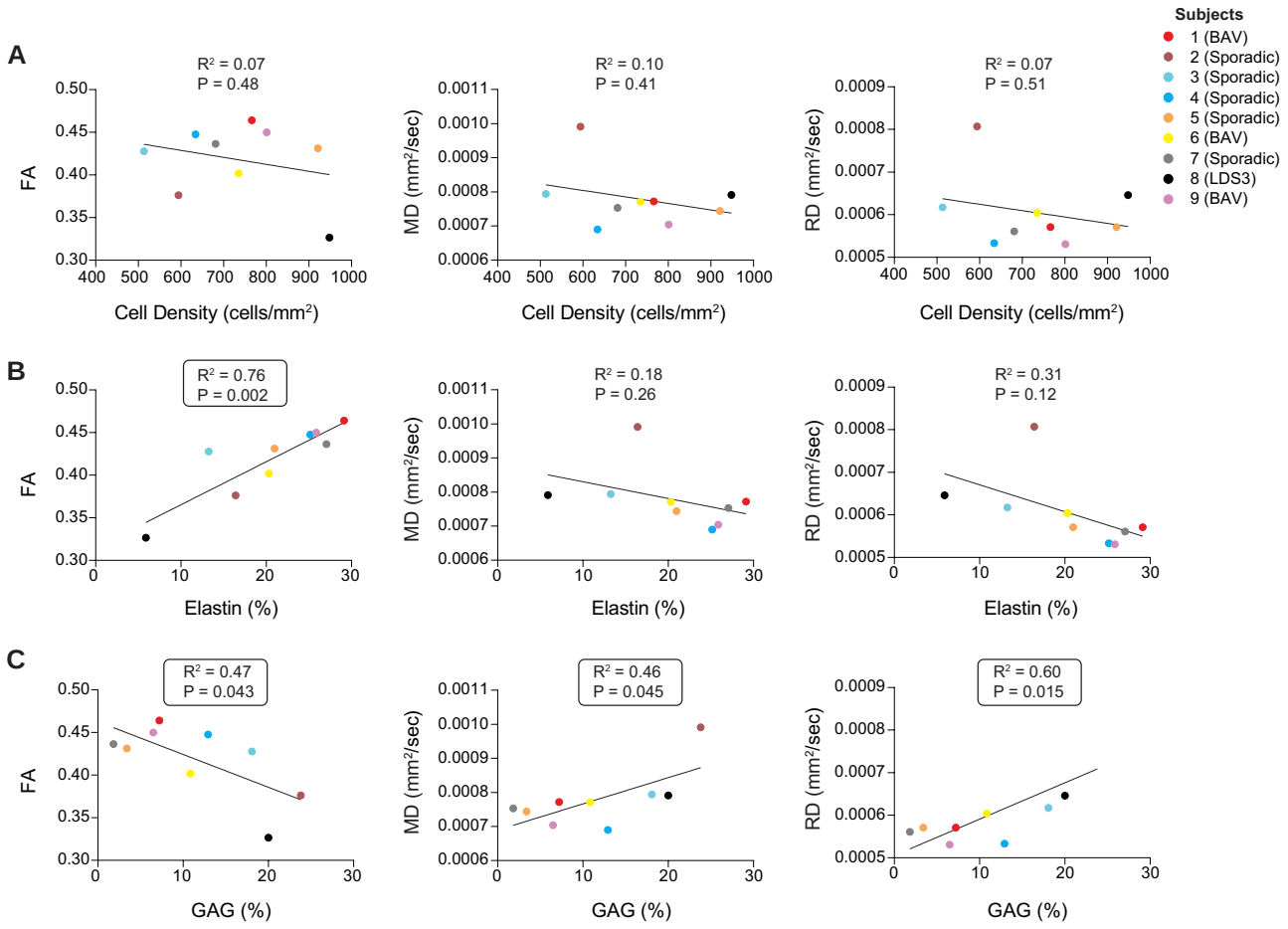

Figure 6 Relationships between diffusion tensor imaging metrics and aortic medial composition among subjects undergoing ascending aortic surgery. Scatter plots and linear regression lines depicting the relationships between diffusion tensor imaging metrics and each of smooth muscle cell density (*A*), elastin content (*B*), and glycosaminoglycan content (*C*). The histological attributes are expressed as the average of 30 equally distributed regions of interest (250 μm × 250 μm) in each section, for each patient. The diffusion tensor imaging metrics are slice-averaged values from the magnetic resonance imaging slice containing the section used for histological quantification. FA, fractional anisotropy; MD, mean diffusivity; RD, radial diffusivity; GAG, glycosaminoglycan; BAV, bicuspid aortic valve; LDS3, Loeys-Dietz syndrome 3.

not quantified in that study and the magnitude of DTI differences was relatively small.[26] Our findings in human tissue are noteworthy because biomechanical studies have shown that resistance to delamination is weaker in the inner media than the outer media,[27] suggesting a potential relationship between DTI metrics and propensity to aortic dissection.

A desired attribute of imaging biomarkers is the ability to discriminate inter-individual differences, not only between those with and without disease but also among subjects with disease. To our knowledge, our study provides the first evidence that an imaging strategy can resolve microarchitectural features of the aortic media to the extent that inter-individual differences among TAA aortas could be found. These differences, observed in a sequentially harvested series of ascending aortas, were detected based on slice-averaged DTI signals, an assessment approach that could be suited to translation.

The potential for DTI metrics to inform on specific histopathologic features of the diseased ascending aorta constitutes an exciting paradigm. Interestingly, we found that the most robust associations with DTI metrics were with GAG content. Glycosaminoglycan accumulation is a hallmark of human aneurysmal disease[7] but cannot be modelled with a digestion strategy. Even in animal models of thoracic aortic disease, GAG accumulation is relatively modest.[9] However, in human ascending TAAs, GAGs form large, water-retaining aggregates, expanding the inter-lamellar spaces and occupying zones where elastin, collagen, and SMCs have been lost. Importantly, GAGs confer little to no resistance to disruptive haemodynamic forces and may themselves promote inter-lamellar delamination as they swell.[14,28,29] We recently proposed that non-destructive GAG imaging could be a strategy for assessing TAA risk and reported that chemical exchange saturation transfer (CEST) MRI could identify and localize GAG deposition in human ascending TAA samples.[30] The current findings reveal that DTI, an MRI strategy distinct from CEST MRI, is also sensitive to the accumulation of this pathophysiologically important extracellular matrix (ECM) and raise new prospects for its consideration as a clinical biomarker.

The relationship between DTI metrics and elastin content is also noteworthy. For this ECM constituent, we found that FA was the most consistently associated metric, correlating with elastin content in the porcine model, intra-medial human assessment, and inter-patient assessment. Importantly, elastin is not a dominant source of water movement, and thus, its association with altered DTI metrics could

be indirect. That is, loss of elastin might be a marker of disordered diffusion but not a direct cause. This is consistent with a recent study of cadaveric atherosclerotic carotid arteries where a correlation between FA and elastin content was found. Because there are few to no elastin fibres in the growing intimal atherosclerotic lesion, the correlation in this case may reflect the burden of atherosclerotic plaque.[23] In contrast, TAAs generally do not carry an atherosclerotic burden. Here, elastin lamellae within the media might promote anisotropic water diffusion by acting as guardrails for diffusion of water within other constituents, including GAGs. As such, elastin degradation in TAAs could exacerbate non-directed diffusion within the media.

Smooth muscle cells themselves are also likely key determinants of DTI signals. In the heart, cardiomyocyte organization and packing impact DTI signals.[31] Similar associations may exist with SMCs in the artery wall. Recent studies of decellularized porcine carotid artery support the importance of SMCs in determining DTI signals.[19] We found in both the porcine and the non-aneurysmal human aorta that FA, MD, and RD each correlated with SMC content. However, we did not find a relationship between SMC content and any of the DTI biomarkers when assessing different human aortas. This discordance could reflect the relatively small subject sample size and the narrower range of SMC densities among human disease aortas compared with the porcine model. However, we speculate the discordance also underscores the complex pathology of human TAAs. Although SMC loss is well described in TAAs, overall SMC number can also increase in TAAs.[8] Furthermore, as the ECM architecture is destroyed, SMCs can become less elongated and less aligned. These scenarios could limit the extent to which SMC content correlates with DTI indices.

Taken together, we propose the following paradigm for DTI-detectable aortic medial signals. In the relatively healthy ascending aorta, directionally restricted diffusion within SMCs is the dominant determinant of constrained and directionally organized DTI signals. Aligned SMCs thereby give rise to the diffusion tracts we and others have reported.[17,18] In contrast, in the degenerating aorta, the magnitude and preferred directionality of diffusion can be altered by one or more of the following: (i) loss of SMCs; (ii) disoriented, morphologically altered SMCs; (iii) loss of elastin; and (iii) accumulation of GAGs. We propose that the minimal diffusion constraints of GAG pools are particularly important. Nonetheless, by capturing a range of microarchitectural pathologies, DTI may provide a powerful readout of aortic wall disorder.

We did not identify associations between DTI metrics and aortic diameter, although positive trends for MD and RD were suggested. The lack of significant associations may reflect the small sample size and the complex relationships between medial composition and aortic diameter. In this regard, it is interesting that we found abnormal DTI metrics in diseased aortas that were not substantially dilated, including from a patient with LDS3. Here, there was reduced FA together with GAG accumulation. This is intriguing recognizing that the familial LDS aortopathies are at risk for dissection at relatively smaller dimensions.[32] A larger series is required to determine if DTI can identify those relatively non-dilated aortas that may nonetheless be structurally altered and potentially high risk.

Limitations and future prospects

The enzyme-mediated digestion strategy employed for the porcine aorta analysis differs from the chronic degradation that proceeds in human TAAs in its rapidity and in not capturing cell and ECM remodelling responses. However, the model did entail key pathological changes of TAAs enabling us to elucidate the relationship between specific compositional changes in the aortic wall and DTI signals. As such, it was a compositional analysis tool rather than a model of the disease *per se*. The approach could also set the stage for investigating DTI in large animal models of TAAs, as acute enzyme-mediated aortic wall degeneration strategies have been reported.[33,34] We also note that not all cells in the human aortic media will be SMCs. Inflammatory cells and microvascular endothelial cells, although a minority, could impact water diffusion differently from SMCs. As well, we have not quantified collagen content. Collagen fibres can be disrupted in TAAs[35] although recent studies have suggested arterial collagen only modestly contributes to DTI metrics.[19,20] Also, whereas the porcine aortas were imaged in a fresh state, the human aortas were fixed in formalin. The latter were all subjected to relatively short-term fixation (≤3weeks) ensuring reliable comparisons among them.[36,37]

Imaging the microstructure of the diseased aorta is at an early stage.[38] In this context, the *ex vivo* studies undertaken here using 9.4 T field strength provide an important advance by establishing that degenerative processes in the ascending aorta can be interrogated by DTI. As such, our findings argue for *in vivo* DTI studies of TAAs. However, clinical imaging is done at 3 T or lower field strengths that afford less information content due to the lower spatial resolution and lower signal-to-noise ratio. In addition, unlike the brain, the aorta is a thin-walled structure that moves due to cardiac ejection and respiration. Thus, there are hurdles to overcome for clinical translation of compositional imaging of the aortic wall. It is nonetheless encouraging that there are preliminary reports of *in vivo* DTI of the carotid artery[39] and several *in vivo* studies of cardiac DTI.[31] As well, ongoing technical advances for cardiac imaging, including strategies to reduce the number of breath holds,[40] also hold promise for thoracic aorta imaging.

Conclusions

We have established that *ex vivo* high-field-strength DTI can detect a wide spectrum of damage in the ascending aortic media and can characterize human ascending TAAs in accordance with their histopathology. Loss of elastin and GAG accumulation were particularly well captured by DTI biomarkers. This window into microstructural disorder, and the associated biomechanical implications, raises prospects for probing the risks of TAAs beyond lumen dimensions.

Lead author biography

Mofei Wang is a PhD candidate at the Department of Biochemistry, Western University, Canada. His research interest is thoracic aortic diseases. He takes a transdisciplinary approach including molecular, cellular, and advanced magnetic resonance imaging strategies. He graduated from Western University with an Honours Bachelor of Medical Sciences degree in 2021.

Data availability

The data underlying this article will be shared upon reasonable request to the corresponding author.

Supplementary material

Supplementary material is available at *European Heart Journal Open* online.

Funding

This work was supported by the Canadian Institutes of Health Research (FDN-143326 and PJT-180604; J.G.P.); the Marfan Foundation (J.G.P.,

M.W.A.C., and R.B.); and the Natural Sciences and Engineering Research Council of Canada (RGPIN-2020-05646; R.B. and J.G.P.). J.G.P. holds the Neil McKenzie Chair in Cardiac Care at the Schulich School of Medicine and Dentistry, Western University. M.W.A.C. holds the Ray and Margaret Elliott Chair in Surgical Innovation at the Schulich School of Medicine and Dentistry, Western University.

Conflict of interest: None declared.

References

1. LeMaire SA, Russell L. Epidemiology of thoracic aortic dissection. *Nat Rev Cardiol* 2011; **8**:103–113.
2. Elefteriades JA, Farkas EA. Thoracic aortic aneurysm clinically pertinent controversies and uncertainties. *J Am Coll Cardiol* 2010;**55**:841–857.
3. Groenink M, Koolbergen DR. Surgical treatment of Marfan syndrome and related disorders is all about dealing with uncertainties. *Heart* 2018;**104**:454–455.
4. Sun JCJ. Genetic disorders of the thoracic aorta and indications for surgery. *Cardiol Clin* 2017;**35**:317–320.
5. Pape LA, Tsai TT, Isselbacher EM, Oh JK, O'Gara PT, Evangelista A, Fattori R, Meinhardt G, Trimarchi S, Bossone E, Suzuki T, Cooper JV, Froehlich JB, Nienaber CA, Eagle KA. International Registry of Acute Aortic Dissection I. Aortic diameter > or = 5.5 cm is not a good predictor of type A aortic dissection: observations from the International Registry of Acute Aortic Dissection (IRAD). *Circulation* 2007;**116**:1120–1127.
6. Boodhwani M, Andelfinger G, Leipsic J, Lindsay T, McMurtry MS, Therrien J, Siu SC, Canadian Cardiovascular S. Canadian Cardiovascular Society position statement on the management of thoracic aortic disease. *Can J Cardiol* 2014;**30**:577–589.
7. Halushka MK, Angelini A, Bartoloni G, Basso C, Batoroeva L, Bruneval P, Buja LM, Butany J, d'Amati G, Fallon JT, Gallagher PJ, Gittenberger-de Groot AC, Gouveia RH, Kholova I, Kelly KL, Leone O, Litovsky SH, Maleszewski JJ, Miller DV, Mitchell RN, Preston SD, Pucci A, Radio SJ, Rodriguez ER, Sheppard MN, Stone JR, Suvarna SK, Tan CD, Thiene G, Veinot JP, van der Wal AC. Consensus statement on surgical pathology of the aorta from the Society for Cardiovascular Pathology and the Association For European Cardiovascular Pathology: II. Noninflammatory degenerative diseases—nomenclature and diagnostic criteria. *Cardiovasc Pathol* 2016;**25**:247–257.
8. Yousef S, Matsumoto N, Dabe I, Mori M, Landry AB, Lee SR, Kawamura Y, Yang C, Li G, Assi R, Vallabhajosyula P, Geirsson A, Moeckel G, Humphrey JD, Tellides G. Quantitative not qualitative histology differentiates aneurysmal from nondilated ascending aortas and reveals a net gain of medial components. *Sci Rep* 2021;**11**:13185.
9. Watson A, Nong Z, Yin H, O'Neil C, Fox S, Balint B, Guo L, Leo O, Chu MWA, Gros R, Pickering JG. Nicotinamide phosphoribosyltransferase in smooth muscle cells maintains genome integrity, resists aortic medial degeneration, and is suppressed in human thoracic aortic aneurysm disease. *Circ Res* 2017;**120**:1889–1902.
10. Li G, Wang M, Caulk AW, Cilfone NA, Gujja S, Qin L, Chen PY, Chen Z, Yousef S, Jiao Y, He C, Jiang B, Korneva A, Bersi MR, Wang G, Liu X, Mehta S, Geirsson A, Gulcher JR, Chittenden TW, Simons M, Humphrey JD, Tellides G. Chronic mTOR activation induces a degradative smooth muscle cell phenotype. *J Clin Invest* 2020;**130**:1233–1251.
11. Clement M, Chappell J, Raffort J, Lareyre F, Vandestienne M, Taylor AL, Finigan A, Harrison J, Bennett MR, Bruneval P, Taleb S, Jorgensen HF, Mallat Z. Vascular smooth muscle cell plasticity and autophagy in dissecting aortic aneurysms. *Arterioscler Thromb Vasc Biol* 2019;**39**:1149–1159.
12. Ikonomidis JS, Jones JA, Barbour JR, Stroud RE, Clark LL, Kaplan BS, Zeeshan A, Bavaria JE, Gorman JH III, Spinale FG, Gorman RC. Expression of matrix metalloproteinases and endogenous inhibitors within ascending aortic aneurysms of patients with Marfan syndrome. *Circulation* 2006;**114**:I365–I370.
13. Ghadie NM, St-Pierre JP, Labrosse MR. The contribution of glycosaminoglycans/proteoglycans to aortic mechanics in health and disease: a critical review. *IEEE Trans Biomed Eng* 2021;**68**:3491–3500.
14. Humphrey JD. Possible mechanical roles of glycosaminoglycans in thoracic aortic dissection and associations with dysregulated transforming growth factor-β. *J Vasc Res* 2013; **50**:1–10.
15. Le Bihan D. Looking into the functional architecture of the brain with diffusion MRI. *Nat Rev Neurosci* 2003;**4**:469–480.
16. Tournier JD, Mori S, Leemans A. Diffusion tensor imaging and beyond. *Magn Reson Med* 2011;**65**:1532–1556.
17. Flamini V, Kerskens C, Simms C, Lally C. Fibre orientation of fresh and frozen porcine aorta determined non-invasively using diffusion tensor imaging. *Med Eng Phys* 2013;**35**: 765–776.
18. Flamini V, Creane AP, Kerskens CM, Lally C. Imaging and finite element analysis: a methodology for non-invasive characterization of aortic tissue. *Med Eng Phys* 2015;**37**:48–54.
19. Tornifoglio B, Stone AJ, Johnston RD, Shahid SS, Kerskens C, Lally C. Diffusion tensor imaging and arterial tissue: establishing the influence of arterial tissue microstructure on fractional anisotropy, mean diffusivity and tractography. *Sci Rep* 2020;**10**:20718.
20. Shahid SS, Johnston RD, Smekens C, Kerskens C, Gaul R, Tornifoglio B, Stone AJ, Lally C. Exploring arterial tissue microstructural organization using non-Gaussian diffusion magnetic resonance schemes. *Sci Rep* 2021;**11**:22247.
21. Opriessnig P, Silbernagel G, Krassnig S, Reishofer G. Magnetic resonance microscopy diffusion tensor imaging of collagen fibre bundles stabilizing an atherosclerotic plaque of the common carotid artery. *Eur Heart J* 2018;**39**:3337.
22. Akyildiz AC, Chai CK, Oomens CWJ, van der Lugt A, Baaijens FPT, Strijkers GJ, Gijsen FJH. 3D fiber orientation in atherosclerotic carotid plaques. *J Struct Biol* 2017;**200**: 28–35.
23. Tornifoglio B, Stone AJ, Kerskens C, Lally C. Ex vivo study using diffusion tensor imaging to identify biomarkers of atherosclerotic disease in human cadaveric carotid arteries. *Arterioscler Thromb Vasc Biol* 2022;**42**:1398–1412.
24. Bankhead P, Loughrey MB, Fernandez JA, Dombrowski Y, McArt DG, Dunne PD, McQuaid S, Gray RT, Murray LJ, Coleman HG, James JA, Salto-Tellez M, Hamilton PW. Qupath: open source software for digital pathology image analysis. *Sci Rep* 2017; **7**:16878.
25. Schindelin J, Arganda-Carreras I, Frise E, Kaynig V, Longair M, Pietzsch T, Preibisch S, Rueden C, Saalfeld S, Schmid B, Tinevez JY, White DJ, Hartenstein V, Eliceiri K, Tomancak P, Cardona A. Fiji: an open-source platform for biological-image analysis. *Nat Methods* 2012;**9**:676–682.
26. Shahid SS, Gaul RT, Kerskens C, Flamini V, Lally C. Quantifying the ultrastructure of carotid arteries using high-resolution micro-diffusion tensor imaging-comparison of intact versus open cut tissue. *Phys Med Biol* 2017;**62**:8850–8868.
27. Pasta S, Phillippi JA, Gleason TG, Vorp DA. Effect of aneurysm on the mechanical dissection properties of the human ascending thoracic aorta. *J Thorac Cardiovasc Surg* 2012; **143**:460–467.
28. Roccabianca S, Ateshian GA, Humphrey JD. Biomechanical roles of medial pooling of glycosaminoglycans in thoracic aortic dissection. *Biomech Model Mechanobiol* 2014;**13**: 13–25.
29. Roccabianca S, Bellini C, Humphrey JD. Computational modelling suggests good, bad and ugly roles of glycosaminoglycans in arterial wall mechanics and mechanobiology. *J R Soc Interface* 2014;**11**:20140397.
30. Mortuza R, Ching-Johnson JA, Yin H, O'Neil C, Cronin AE, Randhawa VK, Nong Z, Hashi AA, Li AX, Bartha R, Chu MWA, Pickering JG. Imaging of glycosaminoglycans in ascending aortic aneurysms with chemical exchange saturation transfer MRI. *JACC Cardiovasc Imaging* 2022;**15**:1670–1672.
31. Khalique Z, Ferreira PF, Scott AD, Nielles-Vallespin S, Firmin DN, Pennell DJ. Diffusion tensor cardiovascular magnetic resonance imaging: a clinical perspective. *JACC Cardiovasc Imaging* 2020;**13**:1235–1255.
32. Van Laer L, Dietz H, Loeys B. Loeys-Dietz syndrome. *Adv Exp Med Biol* 2014;**802**: 95–105.
33. Eckhouse SR, Logdon CB, Oelsen JM, Patel RK, Rice AD, Stroud RE, Wince WB, Mukherjee R, Spinale FG, Ikonomidis JS, Jones JA. Reproducible porcine model of thoracic aortic aneurysm. *Circulation* 2013;**128**:S186–S193.
34. Tian Y, Zhang W, Sun J, Zhai H, Yu Y, Qi X, Jones JA, Zhong H. A reproducible swine model of proximal descending thoracic aortic aneurysm created with intra-adventitial application of elastase. *J Vasc Surg* 2018;**67**:300–308.e2.
35. Balint B, Yin H, Nong Z, Arpino JM, O'Neil C, Rogers SR, Randhawa VK, Fox SA, Chevalier J, Lee JJ, Chu MWA, Pickering JG. Seno-destructive smooth muscle cells in the ascending aorta of patients with bicuspid aortic valve disease. *EBioMedicine* 2019; **43**:54–66.
36. Giannakidis A, Gullberg GT, Pennell DJ, Firmin DN. Value of formalin fixation for the prolonged preservation of rodent myocardial microanatomical organization: evidence by MR diffusion tensor imaging. *Anat Rec (Hoboken)* 2016;**299**:878–887.
37. Lohr D, Terekhov M, Veit F, Schreiber LM. Longitudinal assessment of tissue properties and cardiac diffusion metrics of the ex vivo porcine heart at 7T: impact of continuous tissue fixation using formalin. *NMR Biomed* 2020;**33**:e4298.
38. Rastogi V, Stefens SJM, Houwaart J, Verhagen HJM, de Bruin JL, van der Pluijm I, Essers J. Molecular imaging of aortic aneurysm and its translational power for clinical risk assessment. *Front Med (Lausanne)* 2022;**9**:814123.
39. Opriessnig P, Mangge H, Stollberger R, Deutschmann H, Reishofer G. In vivo cardiovascular magnetic resonance of 2D vessel wall diffusion anisotropy in carotid arteries. *J Cardiovasc Magn Reson* 2016;**18**:81.
40. Ferreira PF, Banerjee A, Scott AD, Khalique Z, Yang G, Rajakulasingam R, Dwornik M, De Silva R, Pennell DJ, Firmin DN, Nielles-Vallespin S. Accelerating cardiac diffusion tensor imaging with a U-net based model: toward single breath-hold. *J Magn Reson Imaging* 2022;**56**:1691–1704.